The Journal of Chemical Physics

Wettability of ultra-small pores of carbon electrodes by size-asymmetric ionic fluids

Cite as: J. Chem. Phys. **152**, 054708 (2020); https://doi.org/10.1063/1.5131450
Submitted: 14 October 2019 . Accepted: 14 January 2020 . Published Online: 03 February 2020

Kun Liu, and Jianzhong Wu

The Journal of Chemical Physics ARTICLE scitation.org/journal/jcp

Wettability of ultra-small pores of carbon electrodes by size-asymmetric ionic fluids

Cite as: J. Chem. Phys. 152, 054708 (2020); doi: 10.1063/1.5131450
Submitted: 14 October 2019 • Accepted: 14 January 2020 •
Published Online: 3 February 2020

Kun Liu and Jianzhong Wu[a)]

AFFILIATIONS

Department of Chemical and Environmental Engineering, University of California, Riverside, California 92507, USA

Note: This paper is part of the JCP Special Topic on Interfacial Structure and Dynamics for Electrochemical Energy Storage.
[a)]**Author to whom correspondence should be addressed:** jwu@engr.ucr.edu

ABSTRACT

Recently, we studied the phase behavior of ionic fluids under confinement using the classical density functional theory within the framework of the restricted primitive model. The theoretical results indicate that narrowing the pore size may lead to a drastic reduction in the electric double layer capacitance, while increasing the surface electrical potential would improve the ionic accessibility of micropores. In this work, we extend the theoretical investigation to systems containing size-asymmetric electrolytes that may exhibit a vapor-liquid like phase transition in the bulk phase. The effects of pore size and surface electric potential on the phase diagram and microscopic structures of the confined electrolytes were studied over a broad range of parameters. We found that decreasing the pore size or increasing the surface potential could destabilize the liquid phase in micropores, and capillary evaporation could occur regardless of the size asymmetry between cations and anions. Compared to that in a symmetric ionic system, the vapor-liquid phase separation is more likely to take place as the size asymmetry becomes more pronounced. The phase transition would alter the "accessibility" of ions to micropores and lead to coexisting micropores with different surface charge densities as identified by Monte Carlo simulation.

I. INTRODUCTION

Porous carbons have been widely used as electrode materials for various electrochemical devices including batteries, electric double layer (EDL) capacitors, and fuel cells.[1] The performance of these energy-storage devices is closely related to the specific surface area of the carbon materials. Whereas conventional EDL models assume a linear dependence of the capacitance on the specific surface area, recent experiments and theoretical studies indicate that the energy and power density are also influenced by the pore geometry and size distributions.[2] Erroneous conclusions might be reached if one would evaluate the performance of EDL capacitors without considering the accessibility of micropores.[3,4] Conventionally, accessibility is loosely defined in terms of pore geometry, viz., a micropore is accessible to solvated or bare ions if its size is larger than the ion diameter. However, such a definition of pore accessibility or electrolyte wettability could be misleading because it implicitly assumes ions as rigid particles and ignores phase transition arising from multi-body correlation effects. Even for pores much larger than the ion diameter, phase separation of the confined ionic fluid may lead to an extremely low ion density inside the pore, thus making a negligible contribution to the EDL performance. The phase separation depends not only on the interaction of ionic species with the pore surface but also on the thermodynamic conditions.[5]

In a previous work,[6] we studied the phase behavior of ionic fluids in a porous electrode using the restricted primitive model (RPM). We demonstrated that capillary evaporation may take place inside a porous electrode when the pore size is comparable to the ion diameter. The phase transition is responsible for a drastic reduction in the EDL capacitance at low electrical potential or when the pore size is reduced to microscopic scales. From a practical perspective, the phase separation will be manifested in terms of demixing of an organic electrolyte in small pores but less likely as the vapor-liquid coexistence of a room temperature ionic liquid (RTIL). Under ambient conditions, the liquid density of a typical RTIL is remote from the saturation density, i.e., from the vapor-liquid phase boundary. The sharp difference between the ion concentration of a typical RTIL and that of an organic electrolyte may explain discrepancies concerning the pore size effects

on the performance of porous carbon electrodes for capacitive energy storage.[7]

While the RPM captures much of the essential physics underpinning electrolyte wettability of micropores, it does not describe size asymmetry between cations and anions that could play a significant role in determining the properties of RTILs or organic electrolytes. The difference in the ion size would affect the phase behavior of the ionic systems including electrolyte demixing under confinement. Over the past two decades, a number of theoretical studies have been devoted to understanding the vapor-liquid-like transition of size-asymmetric ionic systems in the bulk.[8–16] Based on the primitive model (PM) of electrolyte systems, results from molecular simulations indicate that, in suitably defined dimensionless units, the critical temperature falls as the disparity between cations and cations increases. The reduction in the critical temperature can be attributed to the formation of larger clusters with the increased asymmetry of ion size, shape, or valency. The asymmetric effects cannot be captured with conventional theories of ionic fluids such as the Debye-Hückel equation or the mean-spherical approximation (MSA) because they neglect multibody electrostatic correlations responsible for the cluster formation. Qualitatively, the high-order correlation effects can be accounted for with the statistical field theory based on the method of collective variables (CVs).[17] In comparison with simulation results, the field-theoretical description predicts the correct trends for the critical temperature varying with the ion asymmetry. Alternatively, Qin and Prausnitz incorporated MSA with the thermodynamic perturbation theory to account for additional contributions to thermodynamic properties due to the formation of ion pairs.[18] With the electrostatic correlation energy in an asymmetric system approximated by that of a symmetric system using an effective ion diameter, the so-called simplified MSA (sMSA) approach predicts the critical properties of size-asymmetric ionic liquids in reasonable agreement with the simulation results.

In comparison with the bulk systems, ionic fluids under confinement are necessarily more complicated and their phase behavior remains much less understood. Several theoretical approaches have been proposed to study the vapor-liquid transition of ionic fluids confined in the micropores of "simple geometry" or in amorphous porous matrices. These include the classical density functional theory (cDFT),[6,19] the field-theoretical approach,[20] or the scaled-particle theory (SPT).[21] Simulation methods have also been used to examine the phase behavior of inhomogeneous ionic systems.[22–24] The simulation work was primarily concerned with capillary evaporation or the variation of the surface charge with the electrical potential under different solution conditions including asymmetry in ion diameters. Although phase transition was investigated in terms of discontinuity in the surface charge density, the simulation did not predict any phase diagram of confined electrolytes. To our knowledge, the asymmetric effects on the phase transition of confined ionic systems have not been systematically studied before. We expect that, in addition to confinement effects, the phase transition will be strongly influenced by the surface electric potential, an important parameter for electrolytes in porous electrodes. Besides, recent simulation results suggest that a highly asymmetric electrolyte in slit-like pores may be separated into domains of high and low surface charge densities.[22] The phase separation may lead to evaporation of an ionic fluid within a porous electrode, thereby drastically reducing the EDL capacitance.[24]

In this work, we extend our previous study of the vapor-liquid transition of model ionic fluids in porous electrodes by an explicit consideration of the size asymmetry between cations and anions. While such effects were investigated before for bulk ionic systems, it is to our knowledge that this work represents the first comprehensive study of the phase behavior of asymmetric electrolytes in nanopores. In this article, we first introduce cDFT equations that are able to reproduce the qualitative behavior of the asymmetric effect on the critical properties of bulk electrolyte systems. Following Qin and Prausnitz,[18] we take into account the contribution of multibody electrostatic correlations to the thermodynamic properties within the framework of the simplified MSA (sMSA). The ionic fluid is modelled as a mixture of free ions and ion pairs in chemical equilibrium according to the mass action law (MAL). To analyze the size asymmetric effects on the wettability of micropores, we use the cDFT equations to construct the phase diagrams of confined ionic fluids over a broad range of pore sizes and surface electric potentials. The theoretical predictions provide insights into the rich behavior of asymmetric ionic fluids in porous electrodes and a sound basis to understand the thermodynamic stability of electrolytes in electrochemical devices under diverse conditions of confinement.

II. THEORETICAL MODEL AND METHOD

A. Coarse-graining procedure

We consider the primitive model (PM) for ionic fluids with monovalent cations and anions ($Z_+ = -Z_- = 1$). Whereas the simple model lacks atomic details, it allows us to capture electrostatic correlations and excluded volume effects of ionic species in the bulk and under confinement. Importantly, this model provides a semi-quantitative description of the phase behavior of organic electrolytes including room temperature ionic liquids in various organic solvents.[25,26] In dimensionless units, the pair potential between any two ionic species is given by

$$\beta u_{ij} = \begin{cases} \infty, & r < \sigma_{ij} \\ Z_i Z_j l_B / r, & r \geq \sigma_{ij} \end{cases}, \tag{1}$$

where r is the center-to-center distance between ions i and j, σ_i and σ_j are the corresponding hard-sphere diameters, $\sigma_{ij} = (\sigma_i + \sigma_j)j/2$, $\beta = 1/k_B T$, and $l_B = \beta e^2/(4\pi\varepsilon_0\varepsilon)$ is the Bjerrum length. As usual, k_B represents the Boltzmann constant, T is the absolute temperature, e is the unit charge, ε_0 is the vacuum permittivity, and ε is the relative permittivity of the dielectric medium, i.e., the static dielectric constant of the pure solvent (or background) that mediates electrostatic interaction between ionic species at infinitely low density/concentration.

In addition to the valence, the difference between cations and anions is characterized by the size asymmetry parameter,

$$\lambda \ldots \sigma_-/\sigma_+. \tag{2}$$

For $\lambda = 1$, the model reduces to the RPM. Because of the charge symmetry with respect to the exchange of "+" and "−" ions, the theoretical results are convertible for $\lambda > 1$ and $\lambda < 1$. In this study,

we consider only $\lambda \leq 1$, i.e., the cations are always larger than the anions.

The static dielectric constant appeared in the primitive model should not be confused with that of the bulk ionic system. Whereas the former depends only on the properties of the pure solvent, the latter is also a function of the ion concentration, which can be accounted for by an explicit consideration of ion-solvent interactions.[27–30] If the primitive model is used to represent a room temperature ionic liquid, a "residual" dielectric constant can be introduced to account for the ionic polarizability effects, which also differs from the static dielectric constant of the bulk ionic system.[31] Approximately, the static dielectric constants of common methylimidazolium-based ionic liquids are in the range of 5–40 at room temperature (e.g., 6.5 for 1-octyl-3-methylimidazolium bis(trifluoromethylsulfonyl)imide and 35 for 1-ethyl-3-methylimidazolium ethylsulfate).[32] By contrast, a "residual" dielectric constant between 2 and 5 is sufficient to reproduce the capacitance of the 1-ethyl-3-methylimidazolium bis(trifluoromethylsulfonyl)imide (EMIM-TFSI) ionic liquid in carbon electrodes.[7] For organic electrolytes exhibiting liquid-liquid demixing near room temperature. The size ratio of ionic species varies approximately from $\lambda = 0.2$–1, and the dielectric constants of the organic solvents are typically in the range between 2 and 25 at the critical temperature. It has been shown that the phase diagrams can be reasonably represented by the primitive model.[26]

For the model ionic system in a slit pore of width H, each ion experiences an external potential along the normal direction of the planar walls positioned at $z = 0$ and $z = H$,

$$V_i(z) = V_i^{HW}(z) + V_i^{C}(z), \tag{3}$$

where $V_i^{HW}(z)$ represents the hard-wall potential,

$$V_i^{HW}(z) = \begin{cases} \infty, & z < \sigma_i/2 \quad \text{or} \quad z > H - \sigma_i/2 \\ 0, & \text{otherwise} \end{cases}, \tag{4}$$

and $V_i^{C}(z)$ the direct electrical potential between an ion of species i and the planar walls,

$$\beta V_i^{C}(z) = -2\pi l_B Z_i H Q/e, \tag{5}$$

where Q stands for the surface charge density on *each* wall. Whereas the discontinuity between the dielectric constants of the porous electrode and the electrolyte may also play a role in determining the ionic distributions and thermodynamic properties,[33] we assume that the image charge effects due to the inhomogeneity of the dielectric medium will not change the qualitative behavior of the phase diagrams.

Schematically, Fig. 1 shows the model ionic system investigated in this work. For convenience, the cation diameter σ_+ is fixed and used as the unit length, i.e., $\sigma \equiv \sigma_+$ is used as the length scale. The pore width and distance from a slit pore surface are thus given in terms of dimensionless units as $H^* = H/\sigma$ and $z^* = z/\sigma$. The dimensionless local electrical potential is defined as $\psi^* = \beta\psi e$, where ψ stands for the local electrical potential due to all charges [see Eq. (7)], and the dimensionless charge density at the surface of the slit pore is defined as $Q^* = Q\sigma^2/e$.

Because of capillary evaporation, an ionic liquid stable in the bulk may exist in a slit pore either as a liquid or a vapor-like phase

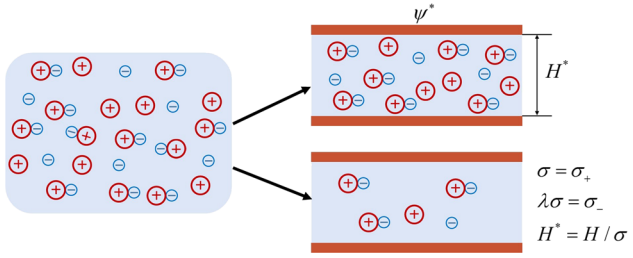

FIG. 1. Schematic of phase separation for an ionic fluid in a slit pore of reduced width $H^* = H/\sigma$ and reduced surface electrical potential $\psi^* = \beta\psi e$.

(or equivalently, electrolytes of high and low ion concentrations). The phase transition occurs when the confined liquid and the confined vapor have the same chemical potential and the same grand potential.[34] It should be noted that the phase behavior of confined ionic systems described in this work is entirely different from that reported by Palmeri and co-workers for aqueous electrolytes.[20,35,36] While an organic electrolyte may exhibit demixing even without the confinement effects, phase transition in an aqueous electrolyte is possible only under extreme confinement such that the local dielectric constant is drastically different from that of the bulk water.

B. Classical DFT

As discussed in our previous work,[6] we are interested in "vapor-liquid-like" phase transition in confined ionic systems. Given the chemical potentials of the ionic species corresponding to those for a bulk electrolyte at the same temperature, the coexistence between the vapor and liquid phases can be identified by equaling the grand potential,

$$\Omega[\rho_i^{v}(\mathbf{r})] = \Omega[\rho_i^{l}(\mathbf{r})], \tag{6}$$

where $\rho_i(\mathbf{r})$ stands for inhomogeneous ionic distributions, and superscripts "v" and "l" refer to the vapor and liquid phases, respectively. Intuitively, the confined ionic system may be considered to be in equilibrium with the bulk electrolyte because they have the same temperature and ionic chemical potentials. However, the bulk system is immaterial to possible phase transitions in the confined geometry because it only defines the chemical potentials of ionic species. As discussed later, the bulk system may not be even thermodynamically stable. By a comparison of the phase boundaries of the confined and bulk systems at the same ionic chemical potentials, we can predict whether or not the confinement destabilizes an ionic system subject to potential phase transitions. The procedure for phase-equilibrium calculations is in principle exact. However, approximations are inevitable in comparison with realistic ionic systems arising from both the molecular model and from formulation of the grand potential. Those approximations distinguish different versions of cDFT calculations.

Whereas the extension of the cDFT equations reported in our earlier work to account for the size asymmetry between ionic species appears straightforward, the direct application of the "standard" MSA and association models fails to capture the critical properties

of bulk electrolytes even qualitatively. In this work, we took a semi-empirical approach by reformulating the Helmholtz energy due to electrostatic correlations in terms of that for size-symmetric ionic systems (RPM) with an effective diameter. A similar approach was used by Qin and Prausnitz for describing the phase behavior of asymmetric bulk electrolyte systems.[18]

For ions in a slit pore, the external potential and the ionic density profiles vary only in the z direction, i.e., the direction normal to the planar walls. As a result, the grand potential is given by

$$\Omega = F[\{\rho_i\}] + \frac{1}{2}\sum_{i=+,-} eZ_i \int \rho_i(z)\psi(z)dz + \sum_{i=+,-}\int \rho_i(z)[V_i^{HW}(z) - \mu_i]dz, \quad (7)$$

where $F[\{\rho_i\}]$ stands for the intrinsic Helmholtz energy, $\psi(z)$ is the local electrical potential, which takes into account the surface charge and interactions among mobile charges, and μ_i denotes the chemical potential of ionic species i. In general, $F[\{\rho_i\}]$ can be decomposed into an ideal part and an excess due to inter-particle interactions,

$$F[\{\rho_i\}] = F^{id}[\{\rho_i\}] + F^{ex}[\{\rho_i\}]. \quad (8)$$

For the model system considered in this work, the ideal Helmholtz energy is exactly known,

$$\beta F^{id}[\{\rho_i\}] = \sum_{i=+,-}\int d\mathbf{r}\rho_i(\mathbf{r})\{\ln[\rho_i(\mathbf{r})\Lambda_i^3] - 1\}, \quad (9)$$

where Λ_i denotes the thermal wavelength of particle i, a parameter immaterial to phase-equilibrium calculations. The excess intrinsic Helmholtz energy is related to ion size and electrostatic correlations and can be written as

$$\beta F^{ex}[\{\rho_i\}] = \beta F_{hs}^{ex}[\{\rho_i\}] + \beta F_{el}^{ex}[\{\rho_i\}] + \beta F_{as}^{ex}[\{\rho_i\}], \quad (10)$$

where $F_{hs}^{ex}[\{\rho_i\}]$ represents the Helmholtz energy due to hard-sphere repulsion or ionic excluded volume effects, $F_{el}^{ex}[\{\rho_i\}]$ arises from electrostatic correlations, and $F_{as}^{ex}[\{\rho_i\}]$ accounts for additional contribution due to association between cations and anions. Equation (10) does not include the contribution due to direct Coulomb interactions because that has been accounted for by the term in Eq. (7) related to the mean-electrical potential $\psi(z)$.

As reported in our previous work, the hard-sphere term $F_{hs}^{ex}[\{\rho_i\}]$ is described according to the modified fundamental measure theory (MFMT),[37]

$$\beta F_{hs}^{ex}[\{\rho_i\}] = \int d\mathbf{r}\Phi^{hs}[n_\alpha(\mathbf{r})]. \quad (11)$$

The excess Helmholtz energy density Φ^{hs} depends on scalar and vector weighted densities, $n_\alpha(\mathbf{r})(\alpha = 0, 1, 2, 3)$ and $\mathbf{n}_\alpha(\mathbf{r})(\alpha = V1, V2)$,

$$\Phi^{hs} = -n_0\ln(1-n_3) + \frac{n_1n_2 - \mathbf{n}_{V1}\mathbf{n}_{V2}}{1-n_3} + (n_2^3 - 3n_2\mathbf{n}_{V1}\mathbf{n}_{V2})\frac{n_3 + (1-n_3)^2\ln(1-n_3)}{36\pi n_3^2(1-n_3)^2}. \quad (12)$$

The explicit expressions for the weighted densities and weight functions are available from previous publications. For uniform hard-sphere fluids, MFMT yields an expression for the Helmholtz energy identical to that derived from the Boublik-Mansoori-Carnahan-Starling-Leland (BMCSL) equation of state.[37] Different from the BMCSL equation, MFMT is applicable to uniform as well as inhomogeneous systems. Extensive comparison with Monte Carlo simulation indicates that MFMT provides an accurate description of the structure and thermodynamic properties of inhomogeneous hard-sphere fluids, including those of highly asymmetric hard-sphere mixtures.[37]

For the Helmholtz energy due to electrostatic correlations, we use the reference fluid density (RFD) functional,[38]

$$\beta F_{el}^{ex}[\rho_i(\mathbf{r})] \approx \beta F_{el}^{ex}[\rho_i^{ref}(\mathbf{r})] - \sum_i\int d\mathbf{r}c_i^{(1),el}\Delta\rho_i(\mathbf{r}) - \frac{1}{2}\sum_{i,j}\iint d\mathbf{r}d\mathbf{r}'c_{i,j}^{(2),el}\Delta\rho_i(\mathbf{r})\rho_j(\mathbf{r}'), \quad (13)$$

where $\rho_i^{ref}(\mathbf{r})$ are the density profiles of a locally defined reference fluid, $\Delta\rho_i(\mathbf{r}) = \rho_i(\mathbf{r}) - \rho_i^{ref}(\mathbf{r})$, and $c_i^{(1),\mathrm{el}}$ and $c_{i,j}^{(2),\mathrm{el}}$ are the electrostatic components of the first- and second-order direct correlation functions (DCFs) of the reference fluid, respectively. Since local charge neutrality is everywhere satisfied in the reference system, $c_i^{(1),\mathrm{el}}$ and $c_{i,j}^{(2),\mathrm{el}}$ can be calculated from the MSA for the corresponding bulk fluid. In this work, the contribution from electrostatic correlations in an asymmetric mixture is further approximated by that of a symmetric mixture with effective diameter $\sigma_{ij} = (\sigma_i + \sigma_j)/2$.[18]

Without an explicit consideration of association between cations and anions, the Helmholtz energy functional would reduce to that corresponding to the MSA equations, which fail to capture the size asymmetric effects on the vapor-liquid phase transition of bulk ionic systems. Meanwhile, it has been shown that addition of association between ion pairs provides a more accurate prediction of the critical temperature and the critical density for the restricted primitive model of ionic systems.[39] To remediate the apparent caveat, we add an additional term to account for association between cations and anions,[40]

$$\beta F_{as}^{ex}[\{\rho_i\}] = \int d\mathbf{r}\Phi^{as}[n_\alpha(\mathbf{r})], \quad (14)$$

where the association Helmholtz energy density is given by

$$\Phi_{as}^{ex}(n_\alpha) = \sum_i n_{0,i}\zeta_i\left[\ln\alpha^{(i)}(\mathbf{r}) - \frac{\alpha^{(i)}(\mathbf{r})}{2} + \frac{1}{2}\right]. \quad (15)$$

In Eq. (15), the association Helmholtz energy density is derived using the weighted-density approximation as well. The proportional factor, $\zeta_i = 1 - \mathbf{n}_{V2i}\cdot\mathbf{n}_{V2i}/n_{2i}^2$, takes into account both the scalar- and vector-weighted densities in inhomogeneous systems. This parameter can be understood as the inhomogeneity effects on chemical binding. The parameter $\alpha^{(i)}(\mathbf{r})$ represents the degree of dissociation of species i at position $\mathbf{r}$,

$$\alpha^{(i)}(\mathbf{r}) = \frac{1}{1 + n_{0,j}\zeta_j\alpha^{(j)}(\mathbf{r})\Delta^{ij}(\mathbf{r})}, \quad (16)$$

where $\Delta^{ij}(\mathbf{r}) = K^0 K^r$ represents the association constant, which is approximated by a product of temperature-dependent intrinsic and residual contributions, K^0 and K^r, respectively.

As in the Bjerrum association theory for bulk electrolytes, there is a certain kind of arbitrariness in defining the ion pairs and hence the intrinsic association constant K^0. Ebeling suggested that K^0_{Eb} should reproduce the (osmotic) second virial coefficient of the bulk electrolyte solution.[41] However, Ebeling's approach does not yield satisfactory predictions of the critical properties of the RPM. Following Ref. 42, we choose K^0 in the form proposed by Olaussen and Stell,[43]

$$K^0 \approx 12K^0_{Eb}. \tag{17}$$

On the other hand, K^r is calculated from the simple interpolation scheme (SIS),[44]

$$K^r = y_{\pm}(\sigma), \tag{18}$$

where $y_{\pm}(\sigma)$ is the contact value of the anion-cation cavity correlation function evaluated at $\alpha = 1$, i.e., for the reference ionic fluid without association,

$$y_{\pm} = \left[\frac{1}{1-n_3} + \frac{n_2\sigma_+\sigma_-(1-\mathbf{n}_{V2}\mathbf{n}_{V2}/n_2^2)}{4\sigma_{\pm}(1-n_3)^2}\right] \times \exp\left(-\frac{\Gamma^2 a_+ a_-}{4\pi l_B \sigma_{\pm}}\right)\exp\left(\frac{l_B Z_+ Z_-}{\sigma_{\pm}}\right). \tag{19}$$

Similar to the thermodynamic perturbation theory for bulk systems,[45,46] parameters Γ and a_i can be estimated from the MSA equations,

$$\Gamma^2 = \pi l_B \sum_i \frac{n_{0i}}{(1+\Gamma\sigma_i)^2}\left[Z_i - \frac{\pi P_n \sigma_i^2}{2(1-n_3)}\right]^2, \tag{20}$$

$$a_i = \frac{2\pi l_B\left(Z_i - \frac{\pi P_n \sigma_i^2}{2(1-n_3)}\right)}{\Gamma(1+\Gamma\sigma_i)} \tag{21}$$

with

$$P_n = \sum_i \frac{2n_{1i}Z_i}{1+\Gamma\sigma_i}\Big/\left[1 + \frac{3}{1-n_3}\sum_i \frac{n_{3i}}{1+\Gamma\sigma_i}\right]. \tag{22}$$

III. RESULTS AND DISCUSSION

A. Phase behavior of bulk ionic fluids

We first calibrate the cDFT predictions concerning the effect of size asymmetry between cations and anions on the vapor-liquid diagram of bulk ionic fluids. As shown in Fig. S1, the cDFT equations described above are able to reproduce the qualitative trends on how the critical properties change with the asymmetric parameter λ in comparison with simulation results. While a quantitative description of the critical properties is beyond the scope of this work, we note that the trend was not reproduced by conventional ionic models without an explicit consideration of association between cations and anions.

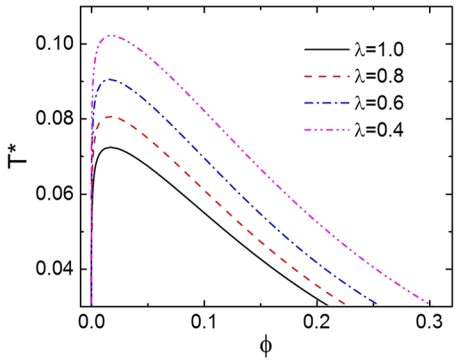

FIG. 2. Phase diagrams for bulk ionic fluids with different cation and anion size ratios. Here, $\lambda = \sigma_-/\sigma_+$, $\phi = \frac{\pi}{6}\sum_i \rho_i \sigma_i^3$ is the ionic packing fraction, and T^* is defined in Eq. (23).

Figure 2 presents the phase diagrams of the bulk ionic fluids with the reduced temperature defined in terms of a fixed cation diameter,

$$T^* = \frac{4\pi\varepsilon_0\varepsilon_r k_B T\sigma}{e^2}, \tag{23}$$

where $\sigma \ldots \sigma_+$. For clarity, we use the diameter of the larger ions as the unit length for defining the reduced temperature so that it varies more significantly with the asymmetric parameter. As the size asymmetry between cations and anions increases, i.e., as λ is reduced from 1 to 0.4, we see a sharp increase in the reduced critical temperature. Qualitatively, the theoretical trend is consistent with the simulation results (Fig. S1). However, the cDFT predictions are about a factor of 2 too high for the critical temperature and a factor of between 2 and 3 too low for the critical density. As revealed by molecular simulations,[9] an increase in the size asymmetry promotes cluster formation, thereby a stronger effective attraction between ionic species. The reduced critical density falls only slightly as the system becomes more asymmetric, which is also consistent with the simulation results. Interestingly, the correct trends would not be reproduced without the assumption of an effective symmetric ionic fluid to account for the electrostatic correlations. The effective diameter $\sigma_{\pm}$ assumption allows us to capture the correct trend for the critical properties because it prohibits the formation of improbable "charge-unbalanced" zones in asymmetric mixtures.[18,47] Similar to typical mean-field theories, the cDFT predictions overestimate the critical temperature in comparison with the simulation data and reproduce the vapor-liquid coexistence curve only semi-quantitatively (Fig. S2).

B. Phase diagrams of asymmetric ionic fluids in neutral pores

An ionic liquid stable in the bulk phase may display a vapor-liquid-like phase transition in a confined geometry. The so-called capillary evaporation depends on, in addition to temperature and pressure of the bulk system, the pore size, surface energy, and electrical potential. If the ionic liquid under confinement exists as a vapor phase, the micropore makes negligible contributions

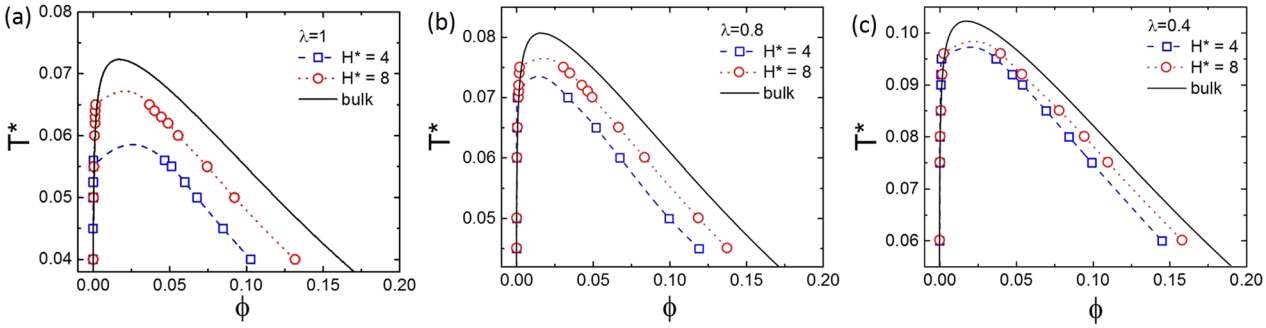

FIG. 3. Phase diagrams for the model ionic fluid in the bulk (solid lines) and in different slit pores with a zero surface electrical potential ($\psi^* = 0$). Here, the anion/cation size ratios are (a) $\lambda = 1$, (b) $\lambda = 0.8$, and (c) $\lambda = 0.4$. The average packing fraction of all ions inside the pore is defined as $\phi = \frac{1}{H}\int dz \frac{\pi}{6}\rho_i(z)\sigma_i^3$. The dashed and dotted lines are added to guide the eye.

to electrochemical performance because of the negligible ionic concentration.

Figures 3(a)–3(c) present the phase diagrams of the model ionic fluids in neutral slit pores for three values of the size asymmetric parameter: $\lambda = 1.0$, 0.8, and 0.4. In all cDFT calculations, the electrical potential at the pore surface is fixed at zero. Similar to our previous report for symmetric ionic systems ($\lambda = 1.0$),[6] the confinement narrows the unstable region of the vapor-liquid phase boundary. Although we did not locate the critical temperatures of the ionic systems in slit pores, it is clear that, in dimensionless units, the critical temperature falls as the pore size decreases. As discussed latter, the smaller pore promotes capillary evaporation provided that the critical temperature of the ionic fluid is above the temperature of the system in a given pore. For the liquid branch of the confined ionic system, the average coexistence density inside the pore is always smaller than the corresponding saturated liquid density in the bulk. However, such a difference is noticeably reduced as the system becomes more asymmetric. For example, at $T^* = 0.06$ and $H^* = 8$, the relative change of the total volume fraction of ions, $(\phi_b - \phi_{confined})/\phi_b$, is 0.300 for $\lambda = 1$ (RPM), and it is reduced to 0.078 for an asymmetric ionic fluid with a size ratio of $\lambda = 0.4$. For bulk ionic fluids, the driving force for the phase transition is the competition between the short range steric repulsion and the attractive correlations arising from the long-range Coulomb interactions.[26,35] For an electrolyte in a slit pore, the phase transition is also influenced by surface interactions including the steric effects. Intuitively, the critical temperature declining with the pore size is understandable because a neutral pore hinders ionic correlations thus compromising effective attraction.

The ionic density profiles provide valuable insights into understanding the properties of the EDL. Near the electrode with zero or a small amount of charge, the effects of size asymmetry on the density distributions have been studied before by both simulation and theoretical studies.[48,49] Figure 4 presents the local ionic densities and the degrees of dissociation for both cations and anions of the confined liquid phase in equilibrium with a vapor in a slit pore of $H^* = 8$. When $\lambda = 1$ and the surface voltage is zero, the local densities of cations and anions are identical [Fig. 4(a)]. As expected, both cations and anions are depleted from the neutral surfaces and the density profiles inside the pore are relatively smooth. The depletion effect can be attributed to the electrostatic correlation effects:[50] an ion interacts more favorable with its full ionic atmosphere in the bulk than with other ions in the vicinity of a neutral surface. The local degree of dissociation, or the fraction of ions exist as

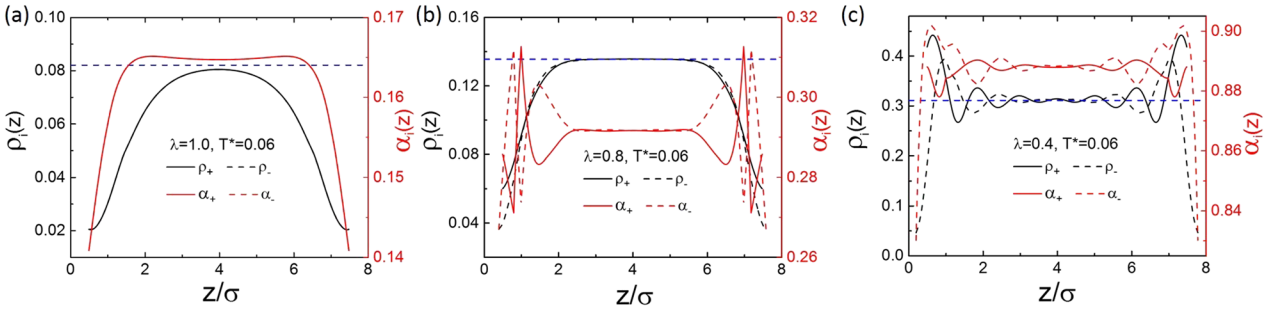

FIG. 4. The density profiles (black solid lines and dashed lines) and the local degree of dissociation (red solid and dashed lines, respectively) of the confined liquids at the vapor-liquid consistence. Here, $H^* = 8$, $T^* = 0.06$, and $\psi^* = 0$. The blue dashed lines represent the bulk number density $\rho_{i,b}$ of (a) 0.082, (b) 0.135, and (c) 0.311, respectively.

monomers, also shows position dependence. It increases from the wall and eventually becomes flat in the middle of the pore, indicating that formation of ion pairs is slightly more favorable near the hard wall than that in the bulk. For the ionic fluids with a size ratio of $\lambda = 0.8$ [Fig. 4(b)], the monomer fraction shows a strong oscillation near the wall. The oscillatory distribution of ions becomes more pronounced for the ionic fluids with the size ratio $\lambda = 0.4$ [Fig. 4(c)].

As shown in Fig. 4(c), anions are depleted from the hard wall because they are smaller than cations, while the local monomer fraction of the anions increases with the distance from the wall and shows an oscillatory behavior similar to that for the density profiles. Interestingly, the local degree of dissociation for cations is smaller than that for anions even though they have a higher local density near the surface.

Figure 4 shows that, in all three cases, associations between monomers are enhanced near the neutral wall due to the reduction in the ion density. At the same temperature, both the saturated liquid density and the degree of dissociation increase as the size asymmetry becomes more pronounced (i.e., as λ becomes smaller). Because a larger density leads to a higher monomer fraction (i.e., a higher degree of dissociation), we conjecture that the formation of ion pairs is prohibited by the excluded volume effects. On the other hand, the more significant the size asymmetry, the less fraction of cations and anions forming ion pairs. It should be noted that the present approach takes into account the association between cations and anions through the formation of ion pairs. Because there is only one association site per molecule of species i, the association model is not able to account for the clustering effects identified by Monte Carlo (MC) simulation for bulk ionic systems.[9,51]

We may compare the stability of the confined ionic fluids relative to that in the bulk at the same chemical potential and temperature. Figure 5 shows the pore size effect on the phase transition of the confined ionic fluids in terms of reduced pressure and reduced chemical potential of the corresponding bulk fluids at $T^* = 0.06$. The chemical potential of the ionic fluid is expressed as a linear combination of μ_i, denoted as $\mu_\pm = (\mu_+ + \mu_-)/2$. At sufficiently high pressure or large chemical potential, the system exists as a liquid state, and at sufficiently low pressure or chemical potential, the system exists as a vapor phase. Here, the lines demarcate the vapor-liquid coexistence for the bulk (dashed lines) and confined systems (solid lines). The cDFT predicts that phase transition inside micropores takes place at a chemical potential higher than that corresponding to the bulk phase, regardless of the pore size and ionic asymmetry. The shift in the chemical potential indicates that an ionic liquid stable in the bulk can be destabilized inside the pore when the pore size becomes sufficiently small.[34]

The confinement effect becomes less important as the pore size increases, and the chemical potential at the vapor-liquid transition of the confined fluid approaches to the bulk limit. Similarly, the pressure corresponding to a bulk liquid with the chemical potential and temperature the same as those of the saturated confined fluid is always higher than the bulk saturation pressure (black dashed lines in Fig. 5). The difference in the saturation pressures of the bulk and confined fluids also indicates that an ionic liquid stable in the bulk phase may experience phase transition inside the pore. While the

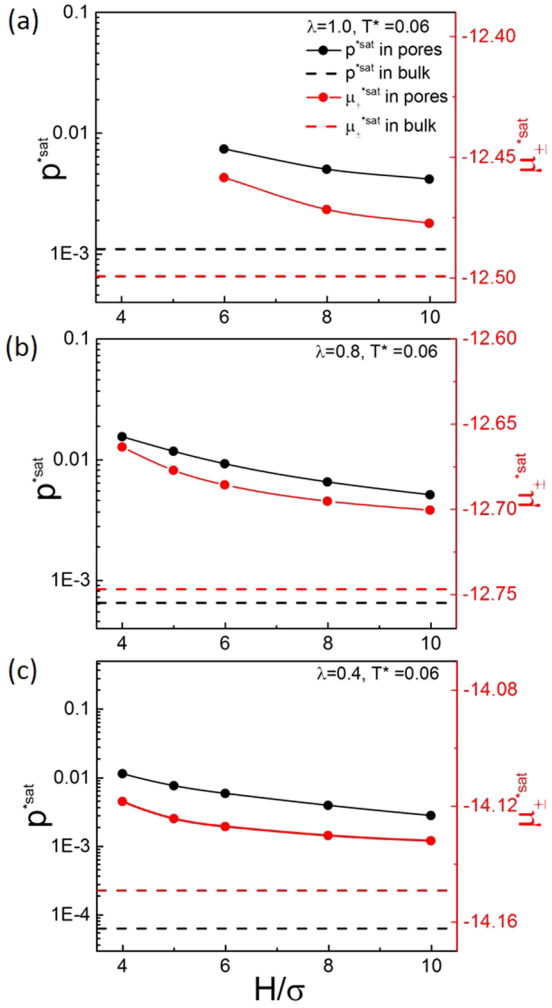

FIG. 5. The reduced pressure ($p^* = \beta p \sigma^3$) and the reduced chemical potential ($\mu_\pm^* = \beta \mu_\pm$) corresponding to the ionic liquid in the bulk phase in contact with the confined ionic system at vapor-liquid equilibrium. In all cases, $T^* = 0.06$ and the different size ratios are (a) $\lambda = 1$, (b) $\lambda = 0.8$, and (c) $\lambda = 0.4$. The black dashed lines represent the saturation pressure for the bulk ionic liquids, and the red dashed lines represent the saturation chemical potentials of the bulk fluids.

saturation pressures of symmetric and asymmetric ionic fluids are about the same order of magnitude (e.g., $p^* = 4.13 \times 10^{-3}$ for $\lambda = 1.0$ and $p^* = 2.79 \times 10^{-3}$ for $\lambda = 0.4$ at $T^* = 0.06$ and $H^* = 10$), the saturation pressure of the symmetric ionic system in the bulk is higher than that of the asymmetric fluid by about two orders of magnitude ($p_{\lambda=1}{}^* = 1.10 \times 10^{-3}$ vs $p_{\lambda=0.4}{}^* = 6.39 \times 10^{-5}$ at $T^* = 0.06$). The drastic difference implies that, at a given thermodynamic condition, an asymmetric ionic liquid is more likely to exist as a vapor phase in the slit pore, and the system becomes more unstable as the ions become more asymmetric. In a slit pore, capillary evaporation depends on the competition between the volume and the surface-energy contributions to the grand potentials of the two coexisting phases.[34]

C. Phase diagrams of asymmetric ionic fluids in charged slit pores

Figure 6 shows the phase diagrams of ionic fluids with size ratios of λ = 1.0, 0.8, 0.6, and 0.4 in a slit pore of reduced width H^* = 4 at different surface voltages. The previous study about the phase diagram of the RPM in slit pores[19] shows that an increase in the surface voltage acts similarly as a decrease in the pore width. However, in the case of the RPM [Fig. 6(a)], the coexistence curves are relatively insensitive to changes in the surface voltage, at least for the pore width considered in this work (i.e., H^* = 4.0). In a narrow pore, the volume effect plays a dominant role in interaction between ions and the electrostatic effect is relatively less important. As the size asymmetry increases (i.e., the decrease in λ), the difference among the phase diagrams with different surface voltages becomes more pronounced. Interestingly, the coexistence curve for a highly asymmetric fluid becomes boarder as the surface voltage increases. In this case, changing the surface voltage has a stronger influence on the phase diagram.

In a previous study,[22] Monte Carlo (MC) simulation was used to investigate the effect of ion size asymmetry on phase transition of electrolytes in idealized porous electrodes. It was found that the surface charge density might be inhomogeneous for a highly asymmetric electrolyte in a slit pore, suggesting phase separation into domains of high and low surface charge densities. Qualitatively, our cDFT predictions shown in Fig. 6 are consistent with the MC results.

We also studied the effect of surface voltage on the phase boundaries of ionic fluids in a slit pore in terms of chemical potentials for the corresponding bulk fluids. Figure 7 shows the reduced chemical potentials of the confined and bulk saturated ionic liquids vs the surface voltage. For all cases, the chemical potential for the confined fluid is more positive than the corresponding chemical potential at the bulk liquid-vapor coexistence, implying a system stable in the bulk may display phase separation in the confined geometry. While the surface voltage stabilizes the liquid phase for the symmetric ionic system, it shows an opposite trend for the size-asymmetric ionic systems [Figs. 7(b)–7(d)]. The ion-surface interaction, especially the Coulomb potential, plays an important role in determining the phase behavior of the confined ionic systems. Due to the size difference between cations and anions, the interfacial structures are remarkably different for symmetric and asymmetric ionic fluids even near a neutral surface.[52] When the ionic fluid is subjected to an external electrical potential, counterions (anion in this study) segregate on the charged surface leading to the formation of layer-by-layer ionic structures sensitive to the size asymmetry of ionic species.[52] The competition between ionic screening and steric interactions is responsible for different effects of the surface electric potential on the phase behavior of symmetric and asymmetric ionic systems. For size-asymmetric ionic fluids, the gap between the confined and bulk coexistence chemical potentials becomes larger as the surface voltage increases, which indicates that the applied voltage destabilizes the liquid phase inside the pore.

Electrosorption of ions in carbon pores has been recognized to affect the performance of capacitive energy storage devices. Experimentally, it was observed that ultra-small pores are not completely wetted at null voltage, but the ion adsorption is strongly enhanced as the surface voltage increases.[53] The pore accessibility can be measured in terms of partition coefficients of ionic species

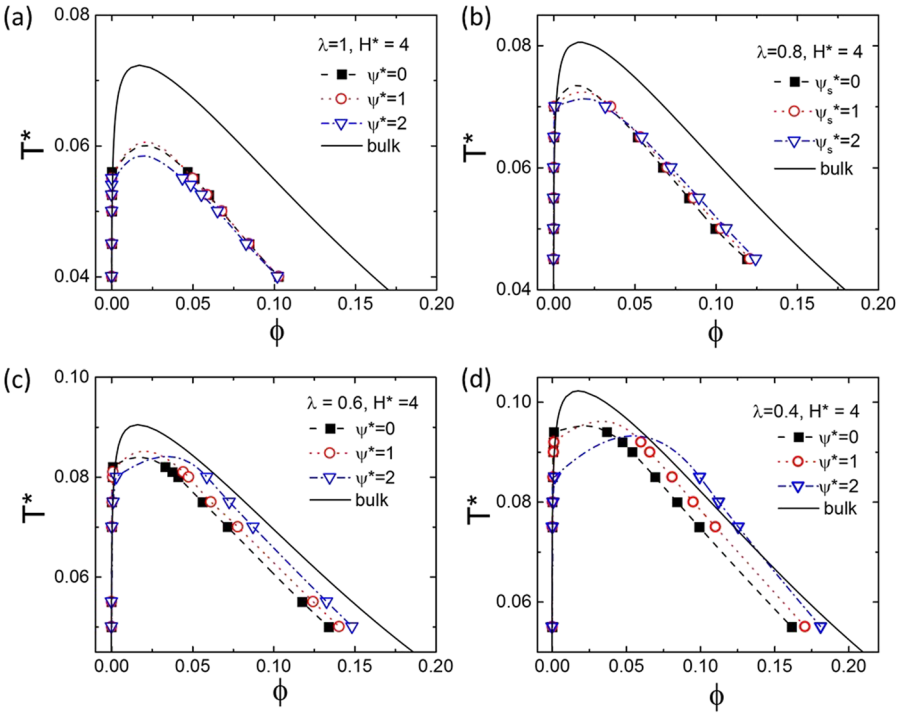

FIG. 6. Phase diagrams of model ionic fluids in a slit pore of H^* = 4 at different surface voltages. Here, the anion/cation size ratios are (a) λ = 1, (b) λ = 0.8, (c) λ = 0.6, and (d) λ = 0.4. The solid lines represent the bulk vapor-liquid coexistence. The dashed, dotted, and dashed-dotted lines are added to guide the eye.

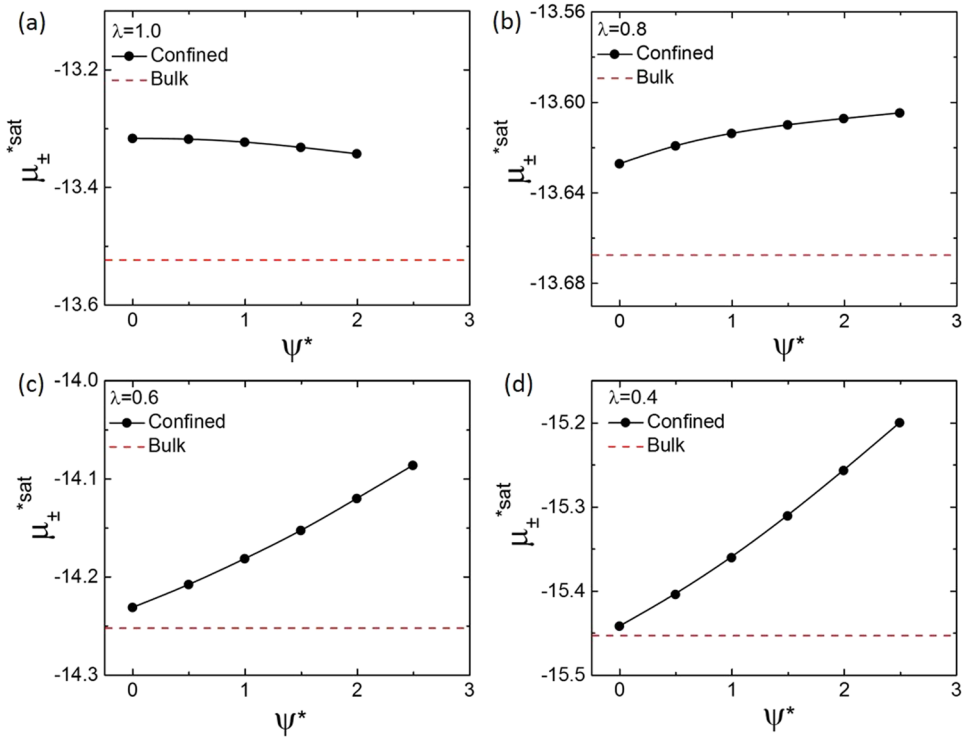

FIG. 7. The reduced chemical potential of the saturated ionic fluids in a slit of H^* = 4 at different surface voltages and size ratios: (a) λ = 1, (b) λ = 0.8, (c) λ = 0.6, and (d) λ = 0.4. In all cases, the reduced temperature is T^* = 0.055, and the solid and dashed lines represent the confined and bulk saturation chemical potentials, respectively.

as a function of pore size.[36] Alternatively, it manifests in the surface charge density, which provides more direct information on the EDL capacitance. In Fig. 8, we analyzed the effects of pore width, applied surface voltages, and bulk ionic density of an asymmetric fluid (λ = 0.4) on ion adsorption in slit pores. Figure 8(a) shows the surface charge density as a function of voltage in slit pores with different pore widths. Here, the temperature is fixed at T^* = 0.0862, which is below the critical temperature of the investigated ionic fluid, and the bulk ionic density is ρ_b^* = 0.17, which is close to the bulk coexisting liquid density at the corresponding temperature. In a large pore (e.g., H^* = 4.0), the surface charge density increases smoothly with the surface voltages, and these pores can be wetted by the ionic fluids at zero voltage. As the pore width decreases, the confinement effect becomes more dominant in the system, and beyond some threshold value, the surface charge density jumps to a finite value and rises continuously as the voltage is further increased. This pseudo-phase-transition in surface charge is also observed in our previous work for symmetric ionic fluids.[6] Such an observation is similar to the experimental results for ion sorption in carbon pores characterized by *in situ* small angle neutron scattering (SANS).[53]

We define the voltage at which the discontinuity of surface charge density occurs as the "critical" voltage, ψ_c^*. In Fig. 8(b), we can see that, for both ionic fluids, the critical voltage is around 2.6. But the corresponding pore width accessible to ions is different. As the bulk ionic fluid density increases from ρ_b^* = 0.17 to 0.21, the accessible pore width corresponding to the reduced critical voltage decreases from H^* = ~1.8 to ~1.5. The reduction in the critical

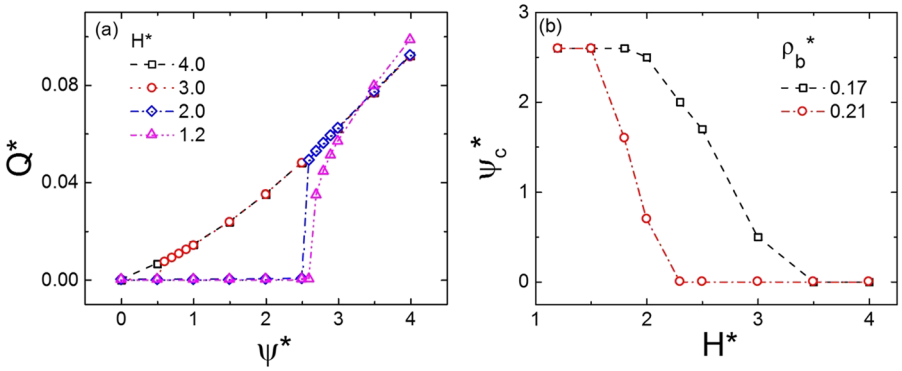

FIG. 8. (a) The surface charge density as a function of surface voltage in slit pores with different widths. Here, the bulk density is $\rho_b^* = \rho_+\sigma_+^3 + \rho_-\sigma_-^3 = 0.17$. (b) The critical surface voltage as a function of pore width. In both cases, the size asymmetric parameter is λ = 0.4 and T^* = 0.0862.

voltage implies that a liquid phase remote from the vapor-liquid coexistence is beneficial for wetting the pore. For an electrolyte with a lower density or concentration, a larger range of pores are "inaccessible" to the ions below the critical voltage.

IV. CONCLUSIONS

In summary, we have developed a coarse-grained model for size-asymmetric ionic fluids and studied its phase behavior in slit pores within the framework of the classical density functional theory (cDFT). By incorporating the association effect between cations and anions, and by using an effective symmetric approximation to account for electrostatic correlations, the cDFT calculations predict correct trends for the size asymmetry effects on the critical parameters of the bulk ionic fluids. We utilized the cDFT method to study the phase behavior of ionic fluids in slit pores both with and without the application of a surface voltage. Similar to the theoretical predictions for symmetric ionic systems, capillary evaporation may take place when the ionic fluids are confined in a neutral or weakly charged slit pore. The theoretical predictions showed that, for highly asymmetric ionic fluids, a vapor-liquid phase transition is more likely to occur in the slit pore. In addition, increasing the surface potential may induce coexisting between micropores of high and low surface charge densities. Qualitatively, the theoretical results are consistent with recent experiments and Monte Carlo simulation for highly asymmetric ionic fluids in the micropores of carbon electrodes. Because capillary evaporation would result in a reduction in the surface charge density, making micropores inaccessible to the underlying ions, the theoretical model provides useful insights into the pore size effects on the performance of various electrochemical devices important for energy storage and other applications of porous carbon.

SUPPLEMENTARY MATERIAL

See the supplementary material for a quantitative comparison of the phase diagrams of the bulk asymmetric electrolytes from theory and simulation and for additional theoretical results on the properties of confined systems.

ACKNOWLEDGMENTS

This work was supported as part of the Fluid Interface Reactions, Structures and Transport (FIRST) Center, an Energy Frontier Research Center funded by the U.S. Department of Energy (DOE), Office of Science, Office of the Basic Energy Sciences. This research used resources of the National Energy Research Scientific Computing Center (NERSC), a DOE Office of Science User Facility supported by the Office of Science of the U.S. Department of Energy.

REFERENCES

[1] G. Wang, L. Zhang, and J. Zhang, Chem. Soc. Rev. **41**, 797 (2012).
[2] C. Lian *et al.*, J. Phys. Chem. C **120**, 8704 (2016).
[3] N. Jackel *et al.*, ACS Energy Lett. **1**, 1262 (2016).
[4] N. Jackel *et al.*, J. Power Sources **326**, 660 (2016).
[5] D. Bonn and D. Ross, Rep. Prog. Phys. **64**, 1085 (2001).
[6] K. Liu, P. Zhang, and J. Wu, J. Chem. Phys. **149**, 234708 (2018).
[7] D. E. Jiang, Z. Jin, and J. Wu, Nano Lett. **11**, 5373 (2011).
[8] J. M. Romero-Enrique *et al.*, Phys. Rev. Lett. **85**, 4558 (2000).
[9] Q. Yan and J. J. de Pablo, Phys. Rev. Lett. **86**, 2054 (2001).
[10] Q. Yan and J. J. de Pablo, Phys. Rev. Lett. **88**, 095504 (2002).
[11] Y. C. Kim, M. E. Fisher, and A. Z. Panagiotopoulos, Phys. Rev. Lett. **95**, 195703 (2005).
[12] W. Zhou and J. K. Percus, Phys. Rev. Lett. **95**, 235701 (2005).
[13] M. Malvaldi and C. Chiappe, J. Phys.: Condens. Matter **20**, 035108 (2008).
[14] O. V. Patsahan and T. M. Patsahan, Phys. Rev. E **81**, 031110 (2010).
[15] S. Bastea, J. Chem. Phys. **135**, 084515 (2011).
[16] C. Desgranges and J. Delhommelle, Chem. Phys. Lett. **687**, 9 (2017).
[17] O. V. Patsahan, T. M. Patsahan, and M. F. Holovko, Phys. Rev. E **97**, 022109 (2018).
[18] Y. Qin and J. M. Prausnitz, J. Chem. Phys. **121**, 3181 (2004).
[19] O. Pizio, A. Patrykiejew, and S. Sokolowski, J. Chem. Phys. **121**, 11957 (2004).
[20] B. Loubet, M. Manghi, and J. Palmeri, J. Chem. Phys. **145**, 044107 (2016).
[21] M. F. Holovko, T. M. Patsahan, and O. V. Patsahan, J. Mol. Liq. **235**, 53 (2017).
[22] K. Kiyohara *et al.*, J. Chem. Phys. **136**, 094701 (2012).
[23] K. Kiyohara *et al.*, J. Chem. Phys. **138**, 234704 (2013).
[24] G. Shrivastav, R. C. Remsing, and H. K. Kashyap, J. Chem. Phys. **148**, 193810 (2018).
[25] M. Martin-Betancourt, J. M. Romero-Enrique, and L. F. Rull, J. Phys. Chem. B **113**, 9046 (2009).
[26] W. Schroer and V. R. Vale, J. Phys.: Condens. Matter **21**, 424119 (2009).
[27] N. Gavish and K. Promislow, Phys. Rev. E **94**, 012611 (2016).
[28] R. A. Persson, Phys. Chem. Chem. Phys. **19**, 1982 (2017).
[29] D. J. Grzetic, K. T. Delaney, and G. H. Fredrickson, Phys. Rev. Lett. **122**, 128007 (2019).
[30] M. Valisko and D. Boda, J. Phys. Chem. B **119**, 14332 (2015).
[31] K. Liu *et al.*, Mol. Phys. **115**, 454 (2017).
[32] T. Singh and A. Kumar, J. Phys. Chem. B **112**, 12968 (2008).
[33] R. Wang and Z. G. Wang, J. Chem. Phys. **139**, 124702 (2013).
[34] R. Roth and K. M. Kroll, J. Phys.: Condens. Matter **18**, 6517 (2006).
[35] S. Buyukdagli, M. Manghi, and J. Palmeri, Phys. Rev. Lett. **105**, 158103 (2010).
[36] S. Buyukdagli, M. Manghi, and J. Palmeri, J. Chem. Phys. **134**, 074706 (2011).
[37] Y. X. Yu and J. Z. Wu, J. Chem. Phys. **117**, 10156 (2002).
[38] D. Gillespie, W. Nonner, and R. S. Eisenberg, J. Phys.: Condens. Matter **14**, 12129 (2002).
[39] J. W. Jiang *et al.*, J. Chem. Phys. **116**, 7977 (2002).
[40] Y. X. Yu and J. Z. Wu, J. Chem. Phys. **116**, 7094 (2002).
[41] W. Ebeling and M. Grigo, J. Solution Chem. **11**, 151 (1982).
[42] M. Holovko, T. Patsahan, and O. Patsahan, J. Mol. Liq. **228**, 215 (2017).
[43] K. Olaussen and G. Stell, J. Stat. Phys. **62**, 221 (1991).
[44] G. Stell and Y. Q. Zhou, J. Chem. Phys. **91**, 3618 (1989).
[45] J. W. Jiang *et al.*, Mol. Phys. **99**, 1121 (2001).
[46] Z. Li and J. Wu, J. Phys. Chem. B **110**, 7473 (2006).
[47] D. M. Zuckerman, M. E. Fisher, and S. Bekiranov, Phys. Rev. E **64**, 011206 (2001).
[48] M. Valisko, D. Henderson, and D. Boda, J. Phys. Chem. B **108**, 16548 (2004).
[49] M. Holovko and D. di Caprio, J. Chem. Phys. **128**, 174702 (2008).
[50] R. Wang and Z. G. Wang, J. Chem. Phys. **142**, 104705 (2015).
[51] Q. L. Yan and J. J. de Pablo, J. Chem. Phys. **114**, 1727 (2001).
[52] J. Z. Wu *et al.*, Soft Matter **7**, 11222 (2011).
[53] S. Boukhalfa *et al.*, ACS Nano **8**, 2495 (2014).